Molecular Cancer Therapeutics

Utility of the RIG-I Agonist Triphosphate RNA for Melanoma Therapy

Mike W. Helms[1], Kerstin Jahn-Hofmann[1], Felix Gnerlich[1], Christiane Metz-Weidmann[1], Monika Braun[1], Gabriele Dietert[2], Petra Scherer[2], Kaj Grandien[1], Joachim Theilhaber[3], Hui Cao[3], Timothy R. Wagenaar[3], Max M. Schnurr[4], Stefan Endres[4,5], Dmitri Wiederschain[3], Sabine Scheidler[1], Simon Rothenfußer[4,5], Bodo Brunner[1], and Lars M. König[4]

Abstract

The pattern recognition receptor RIG-I plays an important role in the recognition of nonself RNA and antiviral immunity. RIG-I's natural ligand, triphosphate RNA (ppp-RNA), is proposed to be a valuable addition to the growing arsenal of cancer immunotherapy treatment options. In this study, we present comprehensive data validating the concept and utility of treatment with synthetic RIG-I agonist ppp-RNA for the therapy of human cancer, with melanoma as potential entry indication amenable to intratumoral treatment. Using mRNA expression data of human tumors, we demonstrate that RIG-I expression is closely correlated to cellular and cytokine immune activation in a wide variety of tumor types. Furthermore, we confirm susceptibility of cancer cells to ppp-RNA treatment in different cellular models of human melanoma, revealing unexpected heterogeneity between cell lines in their susceptibility to RNA agonist features, including sequence, secondary structures, and presence of triphosphate. Cellular responses to RNA treatment (induction of type I IFN, FasR, MHC-I, and cytotoxicity) were demonstrated to be RIG-I dependent using KO cells. Following ppp-RNA treatment of a mouse melanoma model, we observed significant local and systemic antitumor effects and survival benefits. These were associated with type I IFN response, tumor cell apoptosis, and innate and adaptive immune cell activation. For the first time, we demonstrate systemic presence of tumor antigen–specific CTLs following treatment with RIG-I agonists. Despite potential challenges in the generation and formulation of potent RIG-I agonists, ppp-RNA or analogues thereof have the potential to play an important role for cancer treatment in the next wave of immunotherapy.

Introduction

In recent years, immunotherapy has established itself as an important addition to the current armamentarium of cancer treatments, with a prominent role for immune checkpoint inhibitors (1, 2). However, tumor biology has again proven to be complex and elusive, leaving a large portion of tumors unresponsive to currently available therapeutic options, particularly in the absence of tumor-infiltrating immune cells susceptible for activation (3, 4). New immune targets are emerging, with the group of nucleic acid immune sensors or PRR (pattern recognition receptors) being one of the most promising groups for complementing the available arsenal of immune-activating treatments (5–7). PRRs are an integral part of the innate immune system, triggering antiviral responses involving the production of type I IFNs and proinflammatory cytokines. Members of this group include RIG-I–like receptors (RIG-I and MDA-5; ref. 8), the toll-like-receptor family (TLR) and STING (9). Promising therapeutic approaches targeting PRRs have been developed, but have met significant challenges and so far had limited success as standalone therapies. Among other things, biological differences between preclinical species and humans led to failures in clinical trials based on unexpected toxicity profiles or insufficient efficacy for STING and TLR agonists (7, 10–13).

Among nucleic acid immune sensors, RIG-I (encoded by gene DDX58) stands out as a prime candidate for an agonist treatment approach due to reported dual antitumor effects based on cancer cell–specific apoptosis and systemic immune activation (14–19). Furthermore, RIG-I is expressed and available for activation in both, immune and tumor cells. Different from TLRs and STING, RIG-I has no reported major activity or expression differences between human and mouse, supporting translatability of early preclinical results into clinic. On the basis of the described specificity of ppp-RNA as a ligand for RIG-I binding (20–23), it is assumed to have good potential for clinical development, particularly when generated by chemical synthesis.

Building on the existing literature, we sought to further validate and elucidate the utility of synthetic ppp-RNA RIG-I agonists for

[1]Sanofi R&D, Biologics Research, Frankfurt, Germany. [2]Sanofi R&D, Discovery Pathology, Frankfurt, Germany. [3]Sanofi R&D, Oncology Research, Cambridge, MA. [4]Center of Integrated Protein Science Munich (CIPS-M) and Division of Clinical Pharmacology, LMU University Hospital, Munich, Germany. [5]Einheit für Klinische Pharmakologie (EKLIP), Helmholtz Zentrum Muenchen, Neuherberg, Germany.

Note: Supplementary data for this article are available at Molecular Cancer Therapeutics Online (http://mct.aacrjournals.org/).

Current address for F. Gnerlich: AstraZeneca, Innovative Medicines & Early Development Biotech Unit, Gothenburg, Sweden.

Corresponding Author: Mike W. Helms, Sanofi-Aventis Deutschland GmbH, Industriepark Hoechst, Bldg. H831, Frankfurt 65926, Germany. Phone: 49-69-3051-8220; Fax: 49-69-305-17780; E-mail: mike.helms@sanofi.com

Mol Cancer Ther 2019;18:2343–56

doi: 10.1158/1535-7163.MCT-18-1262

the treatment of human cancer, with melanoma as potential entry indication amenable to intratumoral treatment and well characterized for its response to immune therapeutics (24). To this end, we analyzed human clinical melanoma samples for implications of RIG-I expression, characterized RIG-I agonist treatment response in human and mouse melanoma cell lines (including knockout variants) and performed a broad analysis of RIG-I agonist treatment responses in melanoma tumor models *in vivo*.

Material and Methods

Bioinformatic analysis of clinical datasets from TCGA

For correlation of RIG-I (DDX58) expression with immune cell infiltration, Gene Set Variation Analysis (GSVA; ref. 25) was performed with RNA sequencing data (RNAseq) data of 384 samples from the Cancer Genome Atlas (TCGA) melanoma cohort (26) using gene signatures from various immune cell types, including CD8-positive cytotoxic T (CTL) cells, natural killer (NK) cells, dendritic cells (DC), and type 1 Th (Th1) cells (27). For each cell type, the samples are classified into three groups based on the GSVA scores, including "high" (corresponding to top quartile), "low" (corresponding to bottom quartile), and "intermediate." Expression of *DDX58* gene in each group is then visualized through box plots. Student *t* tests are performed between "high" and "low" groups to determine whether there is a correlation between expression of DDX58 and level of infiltration of various immune cell types, which are indicated by the GSVA scores from a specific immune cell–type signature.

To generate a ranked list of gene products and their correlation with RIG-I expression in melanoma, we calculated Pearson correlation coefficients between the expression of *DDX58* gene and 28 genes that are part of or relevant for RIG-I signaling based on RNAseq data of 384 samples from TCGA melanoma cohort.

Regulated Gene Set Enrichment Analysis

Regulated Gene Set Enrichment Analysis (rGSEA) was performed as described before (28) utilizing the type I IFN signature as described by Surpris and colleagues (ref. 29; Supplementary Table S1). The original data can be accessed at the following link provided by the National Center for Biotechnology Information Gene Expression Omnibus: http://www.ncbi.nlm.nih.gov/geo/query/acc.cgi?acc=GSE50682

Briefly, rGSEA generates an activation estimator (−1 or +1) for the pathway represented by a given geneset, and two continuous enrichment scores CL and CR, which are estimates of the slopes of the cumulative distribution of the ranks of the geneset members against the overall gene population (CL and CR are estimated from the 25th percentiles of the distributions). Large values of CL and/or CR thus correspond to many or most of the regulatees being concentrated among the most upregulated and/or most downregulated genes in the gene expression profile of interest. The overall enrichment score is given by the quantity "$\log_2$C" defined as: $\log_2 C = \text{activation} \times \log_2(\max(CL, CR))$.

Log_2C is the quantity reported in the figures to indicate pathway activation for correlation with specific gene expression, represented by $\log_2(TPM+1)$ gene expression values for the indicated genes.

Cell lines and culture

A-375 (ATCC CRL-1619), A101D (ATCC CRL-7898), A431 (ATCC CRL_1555), HT-144 (ATCC HTB-63), SK-MEL-28 (ATCC HTB-72), and C32 (ATCC CRL-1585) were obtained from ATCC. C8161 was originally described by Sipes and colleagues (30). Murine melanoma cell line B16-F10 (ATCC CRL-6475) was also obtained from ATCC. Cell lines were cultured as recommended by the manufacturer. All cells were used for experiments within 20 passages of initial receipt from source. *Mycoplasma* tests were done routinely every 3 months on all cells in culture using the PCR Mycoplasma Test Kit I/C (Promokine).

siRNAs

Information on oligonucleotides can be found in Table 1. Transfection efficiency control: siRNA Hs DDX58_6 (Qiagen, catalog no. SI03019646), normalization purpose: siRNA LV2 modified. The oligodeoxyribonucleotides #7 and #8 were generated by Ella Biotech (Martinsried, Germany).

Nucleic acid synthesis

Oligoribonucleotides were synthesized on solid phase according to standard phosphoramidite oligomerization methodology (capital letters: RNA, lower-case letters: 2′-OMe-RNA, s: Phosphorothioate). Commercially available 5′-O-(4,4′-dimethoxytrityl)-3′-O-(2-cyanoethyl-N,N-diisopropyl) phosphoramidite monomers of uridine (U, U211040, Sigma-Aldrich), 4-N-acetylcytidine (CAc, C213040, Sigma-Aldrich), 6-N-benzoyladenosine (Abz, A211040, Sigma-Aldrich), and 2-N-isobutyrlguanosine (GiBu, G211040, Sigma-Aldrich) with 2′-O-t-butyldimethylsilyl protected phosphoramidites were used.

2′-O-methyl modifications were introduced using the corresponding phosphoramidites carrying the same protecting groups as the regular building blocks. To introduce phosphorothioate linkages, a 50 mmol/L solution of 3-((dimethylamino-methylidene)amino)-3H-1,2, 4-dithiazole-3-thione (AM Chemicals) in anhydrous acetonitrile/pyridine (1:1 vol/vol) was employed. After cleavage and deprotection, oligoribonucleotides were purified by anion-exchange high-performance liquid chromatography and characterized by LC-MS.

The triphosphates (ppp) were introduced as described by Zlatev and colleagues (31).

To generate the double stranded oligoribonucleotides, equimolar amounts of the complementary strands were mixed and

Table 1. Oligonucleotides used in this study

ID#	Target	Specification	Sequence
1	CO4	Duplex ppp	ss: 5′-pppGCG CUA UCC AGC UUA CGU AG-3′ as: 5′-pppCUA CGU AAG CUG GAU AGC GC-3′
2	CO4	Duplex OH	ss: 5′-GCG CUA UCC AGC UUA CGU AG-3′ as: 5′-CUA CGU AAG CUG GAU AGC GC-3′
3	GFP	Duplex ppp	ss: 5′-pppGCC ACA ACG UCU AUA UCA U-3′ as: 5′-pppAUG AUA UAG ACG UUG UGG C-3′
4	GFP	Duplex OH	ss: 5′-GCC ACA ACG UCU AUA UCA U-3′ as: 5′-AUG AUA UAG ACG UUG UGG C-3′
5	GFP	Hairpin ppp	5′-pppGCC ACA ACG UCU AUA UCA UCU CGA GAU GAU AUA GAC GUU GUG GC-3′
6	GFP	Hairpin OH	5′-GCC ACA ACG UCU AUA UCA UCU CGA GAU GAU AUA GAC GUU GUG GC-3′
7	CO4	Hairpin ppp	5′-pppGCG CUA UCC AGC UUA CGU AGA GCU CUA CGU AAG CUG GAU AGC GC-3′
8	CO4	Hairpin OH	5′-GCG CUA UCC AGC UUA CGU AGA GCU CUA CGU AAG CUG GAU AGC GC-3′
9	–	LV2 Control	ss: 5′-AUc GuA cGu AcC GuC GuA udTsdT-3′ as: 5′-AuA cGA cGG uAc GuA cGA udTsdT-3′

annealed in a 1× PBS buffer. The quality of this annealing was analyzed by LC-MS (32).

Cell transfections and analysis

All cell lines were reverse-transfected with siRNAs complexed with Lipofectamine RNAiMAX transfection reagent (Thermo Fisher Scientific). Twenty-thousand cells/well in a 96-well plate were treated with four replicates per siRNA. Cells or supernatants were further processed for analysis at time points indicated in the respective figures.

Cytokine immunoassay. Supernatants from three biological replicates from the transfected different cell lines were pooled 48 hours after transfection and IP-10 release from human cells was quantified with the Human IP-10 Tissue Culture Kit (Meso Scale Discovery, catalog no. K151AVB-2) according to the manufacturer's protocol. Mouse cells were assayed using the Quantikine Mouse IP-10 assay (R&D Systems, catalog no. MCX100).

qRT-PCR. Total RNA was extracted using the SV 96 Total RNA Isolation System from Promega. Samples were processed according to the manufacturer's protocol including a DNase digest during the procedure. Products for cDNA synthesis were purchased from Thermo Fisher Scientific: Reverse Transcriptase Kit (N8080234) and RNase Inhibitor (N8080119). cDNA synthesis was performed with the final concentration of the following reagents:1 × 10× RT Buffer, 5.5 mmol/L $MgCl_2$, 500 μmol/L dNTPs, 2.5 μmol/L Random Hexamers, 2.5 μmol/L Oligo(dT)16, 0.4 U/μL RNase Inhibitor, 1.25 U/μL Multiscribe RT, and 2.5 ng/μL RNA. Samples were incubated at 25°C for 10 minutes and 42°C for 60 minutes. The reaction was stopped by heating to 95°C for 5 minutes. TaqMan Universal PCR Master Mix (4305719) and the TaqMan Gene Expression Assays Hs01061433_m1, Mm01216860_m1, Hs01124251_g1, Mm00445235_m1, Hs00277188_s1 and Mm00439552_s1 were purchased from Thermo Fisher Scientific. qPCR was performed in technical duplicates with an Applied Biosystems Prism 7900 under the following PCR conditions: 2 minutes at 50°C, 10 minutes at 95°C, 40 cycles with 95°C for 15 seconds, and 1 minute at 60°C. PCR was set up as a simplex PCR detecting the target genes [*DDX58* (RIG-I), *CXCL-10* (IP-10), and *IFNB1*] in one reaction and the reference gene (*RPL37A*) for normalization purpose in a second reaction. The final volume for the PCR reaction was 12.5 μL in a 1× PCR Master Mix, reference primers were used in a final concentration of 50 nmol/L and the probe of 200 nmol/L. Oligonucleotides were synthesized by Sigma or Operon. The $\Delta\Delta C_t$ method was applied to calculate relative expression levels of the target transcripts.

Flow cytometry

The mAbs used are mentioned below. Clone names and conjugates are given in parentheses.

Anti-mouse. CD95 (Jo2; PE-Cy7) and H-2D(b) [MHC-I] (KH95; FITC) were from BD Pharmingen; CD274 [PD-L1] (10F.9G; APC), CD45 (30-F11; BV510), CD4 (RM4-5; BV650), and NK1.1 (PK136; BV421) were from BioLegend; CD4 (GK1.5; AF488), CD8 (53.6.7; PE), and CD69 (H1.2F3; PE-Cy7) were from eBioscience; CD3 (145-2C11; BUV395) and CD19 (ID3; BV711) from BD Biosciences; and H-2Kb OVA Tetramer (PE) and CD8a (KT15; FITC) from MBL.

Anti-human. CD95 (DX2; PE-Cy7), pan HLA-I (W6/32; APC), and CD274 [PD-L1] (29E.2A3) were from BioLegend. Life/Dead IR (Invitrogen) was used to exclude dead cells.

Briefly, cells were washed with FACS buffer (BD Pharmingen) and stained for 30 minutes at 4°C or room temperature in FACS buffer and the respective antibody cocktail. For fixation, the Fix/Perm kit from eBioscience was used. Samples were acquired on the LSRFortessa (BD Biosciences) and analyzed using FlowJo software version 10.2 (Tree Star Inc).

Cell preparation for flow cytometry analysis

Supernatant from cell lines was collected and adherent cells were detached using Accutase treatment (Gibco). Cells were washed once with FACS buffer and then stained for 30 minutes at 4°C in FACS buffer and the respective antibody cocktail. Splenocytes were isolated by passing the spleens through a 70-μm cell strainer, followed by red blood cell lysis using ACK lysis buffer (Thermo Fisher Scientific) for 5 minutes at room temperature. After centrifugation, cells were filtered using a MACS preseparation filter (40 μm) resulting in a single-cell suspension. Cells were counted and stained for FACS analysis according to the protocol (2×10^6 cells/staining). For the analysis of ovalbumin (OVA)-Tetramer–positive CD8 T cells, whole blood was collected 48 hours after last treatment in EDTA tubes. After transfer to Eppendorf vials, 10 μL of OVA-Tetramer was added to the blood and incubated for 20 minutes in the dark at room temperature, followed by an additional incubation for 45 minutes at room temperature with the surface antibody mix. Red blood cells were lysed with RBC lysis buffer (BioLegend) 10 minutes at room temperature, followed by washing steps, fixation, and analysis of the samples on the LSRFortessa flow cytometer.

Generation of RIG-I knockout cell C8161 (human) and B16-F10 (murine) using a CRISPR/Cas9 vector

The GeneArt CRISPR Nuclease Vector with an OFP Reporter Kit (Thermo Fisher Scientific) was used to generate RIG-I knockout human C8161 and murine B16-F10 cells according to the manufacturer's instructions. Briefly, target-specific oligonucleotides (top strand oligo human: 5′- GGGTCTTCCGGATATAATCCGTTTT-3′; bottom strand oligo human: 5′-GGATTATATCCGGAAGACCCCGGTG-3′; top strand oligo murine: 5′-CTACATGAGTTCCTGGCTCGGTTTT-3′; bottom strand oligo murine: 5′-CGAGCCAGGAACTCATGTAGCGGTG-3′) were synthesized by Sigma Life Science. Annealing of both single-stranded oligonucleotides resulted in a double-stranded oligonucleotide with compatible ends for cloning into the GeneArt CRISPR Nuclease Vector that was then ligated into the vector using T4 DNA ligase. The ligated vector was transformed into One Shot TOP10 chemically competent *E. coli* (Thermo Fisher Scientific) and the presence of the double-stranded oligonucleotide insert in positive transformants was confirmed by DNA sequencing.

C8161 and B16-F10 cells were transfected with the respective CRISPR/Cas9 vector and Lipofectamine 3000 (Thermo Fisher Scientific) according to the manufacturer's instructions. Forty-eight hours after transfection, cells were screened for the orange fluorescent protein–positive cell clones and sorted using a BD FACS Melody Cell Sorter (BD Biosciences). Single-cell cloning of transfected C8161 and B16-F10 cells lead to cell clones that were then analyzed for RIG-I protein expression by Western blotting

using RIG-I–specific antibodies LS-C344928 (human, clone Alme-1; BIOZOL) and sc-376845 (murine, D-12; Santa Cruz Biotechnology), respectively. Three selected cell clones of each cell lines, which showed absence of RIG-I protein, were further chosen for genome sequencing to verify the successful knockout of RIG-I. To this end, the region including the target site was amplified by PCR using the following primer sets (forward primer human: 5′- CCAGCCAAGCACACAGTAGA -3′, reverse primer human: 5′- GGGAAACGAAACTAGCCCGA -3′, and forward primer murine: 5′- AGGCAGCTTTTTCATCGGGA -3′, reverse primer murine: 5′- GAGTGATGTTTTCCCCTCGC -3′). PCR products from each clone were ligated into TOPO TA Cloning vectors (Thermo Fisher Scientific). A total of 288 cloned vectors [48 clones each derived from each of 6 subcloned cells (3 human cells and 3 murine cells)] were analyzed by Sanger sequencing to confirm that both alleles were deleted from chromosomes.

Cellular ApoTox-Glo assay

Before cell treatment, siRNAs and hairpin RNAs were diluted to 500 nmol/L in OptiMEM (Thermo Fisher Scientific). Subsequently the siRNAs were transfected in 384-well format using LF RNAiMax (Thermo Fisher Scientific) according to the manufacturer's instructions. Briefly, per well 2.5 μL siRNA were mixed with 0.03 μL Transfection Reagent prediluted in 5 μL OptiMEM and incubated for 20 minutes at room temperature. Subsequently 5 μL siRNA/Transfection Reagent complexes were pipetted to the wells of a 384-well plate (Greiner #781091, black with transparent bottom). Thereafter, 5,000 cells in 20 μL cell culture medium were added to each well. The assay plates were incubated for 68 hours under standard cell conditions. To minimize evaporation effects the plates were covered with Micro-Clime plate lids (Labcyte).

Cell viability and toxicity were analyzed using an Apo-Tox-Glo Assay Kit (G6321, Promega) according to the manufacturer's instructions. In brief, 10 μL of GF-AFC Substrate and 10 μL bis-AAF-R110 Substrate were both added to 2.5 mL Assay Buffer and mixed thoroughly. To each well in the 384-well assay plate, 5 μL of diluted substrates in Assay Buffer were added and the plate incubated for 30 minutes at 37°C. Cell viability was determined by measuring fluorescence at 400(Ex)/505(Em) nm [and cytotoxicity was determined by measuring fluorescence at 485(Ex)/205(Em) nm] using an Infinite M1000 Pro plate reader (Tecan).

Animal studies

All animal experiments were carried out in an AAALAC-certified animal facility in accordance with the German animal welfare law and approved by the local authorities.

For all studies, female C57BL/6J mice (Charles River) were used (10–12 weeks of age) and provided water and chow *ad libitum*. A total of 0.5×10^6 B16-F10 cells each were implanted subcutaneously in 100 μL of serum-free growth medium. Tumor growth was followed by caliper measurements. RNA was complexed for injection with *in vivo* Jet-PEI (Polyplus) at N/P = 6 according to the manufacturer's protocol. Twenty micrograms of RNA was delivered per injection in a total volume of 50 μL. Intratumoral dosing was performed every other day after tumors reached an average size of 150 mm^3. Before the first RNA treatment, tumor-bearing animals were randomized into treatment groups to achieve even tumor size distribution. For cytokine analysis, blood was sampled 6 hours post–intratumoral treatment. At study take down, spleens were extracted for cell isolation and FACS analysis as described. Tumors were formalin-fixed and stained for analysis as described previously. Subcutaneous tumor volume was calculated using the formula: length × $width^2/2$.

Mouse serum cytokine analysis

Fifty microliters of undiluted serum was quantified for IP-10 levels using R&D Systems' Quantikine ELISA kit (catalog no. MCX100) according to the manufacturer's protocol. IL4, IL6, IL10, IFNγ, KC/GRO, and TNFα were measured using 50 μL of 1:4 prediluted serum and the Meso Scale Discovery V-Plex Proinflammatory Panel 1 Mouse Kit (catalog no. K15048G) according to the manual on an MSD Sector 6000 instrument. Quantification of IFNα was done with 25 μL of undiluted serum and applying a custom electrochemiluminescence assay based on MSD's technology. For this assay a rat monoclonal anti-mouse IFNα capture antibody (PBL, catalog no. 22100-1) and a rabbit polyclonal anti-mouse IFNα detection antibody (PBL, catalog no. 32100-1) were used.

Results

Patient sample data support an immune-activating role for RIG-I in human melanoma

Before the initiation of laboratory studies, we analyzed publicly available mRNA expression data (TCGA) with the goal to gather support for a therapeutic RIG-I agonist approach in human cancer, specifically melanoma. To this end, we were able to demonstrate that, within the melanomas contained in the TCGA data collection, there was an overall correlation of intratumoral RIG-I levels and the number of infiltrating immune cells as indicated by specific immune cell–associated expression signatures. When categorizing tumors into "high," "medium," or "low" regarding invasion of particular immune cells, we observed the best correlation between RIG-I (DDX58) levels and Th1 CD4 T cells and DC cell infiltration, while the correlation was weaker for CD8 T cells and NK cells (Fig. 1A). Furthermore, we confirmed that RIG-I expression is correlated with a type I IFN expression signature (as described in ref. 29) in tumors of all tissue origins in the TCGA dataset including skin (Fig. 1B). This correlation was also observed for RIG-I like receptor MDA-5 and downstream transcription factor IRF7. As expected, there was no such correlation of type I IFN signature with the non-ISGs MAVS adaptor protein, IRF3 transcription factor and TBK1, respectively (Supplementary Fig. S1). Finally, we ranked gene products that were coexpressed with RIG-I in the TCGA melanomas based on Pearson correlation coefficients (Supplementary Fig. S2). Among the most closely correlated transcripts, we found both PD-L1 (CD274) and PD-L2 (PDCDLG2), along with several components of the MHC, class I (HLA-B, HLA-C, HLA-E, HLA-F, HLA-H, HLA-A, HLA-L, HLA-G) and NK-cell–associated FCGR3A. Among the IFNs, IFN-B1 and IFN-G were most strongly correlated with RIG-I expression. In line with the described shared correlation with the type I IFN signature, we found IRF7 strongly correlated with RIG-I, but not IRF3. However, the most prominent was the correlation identified with IP-10 (CXCL-10), which is again in line with a RIG-I associated type I IFN inflammatory milieu at the tumor site (Supplementary Fig. S3) These data support the notion that RIG-I expression and signaling may be associated with proinflammatory tumor milieu.

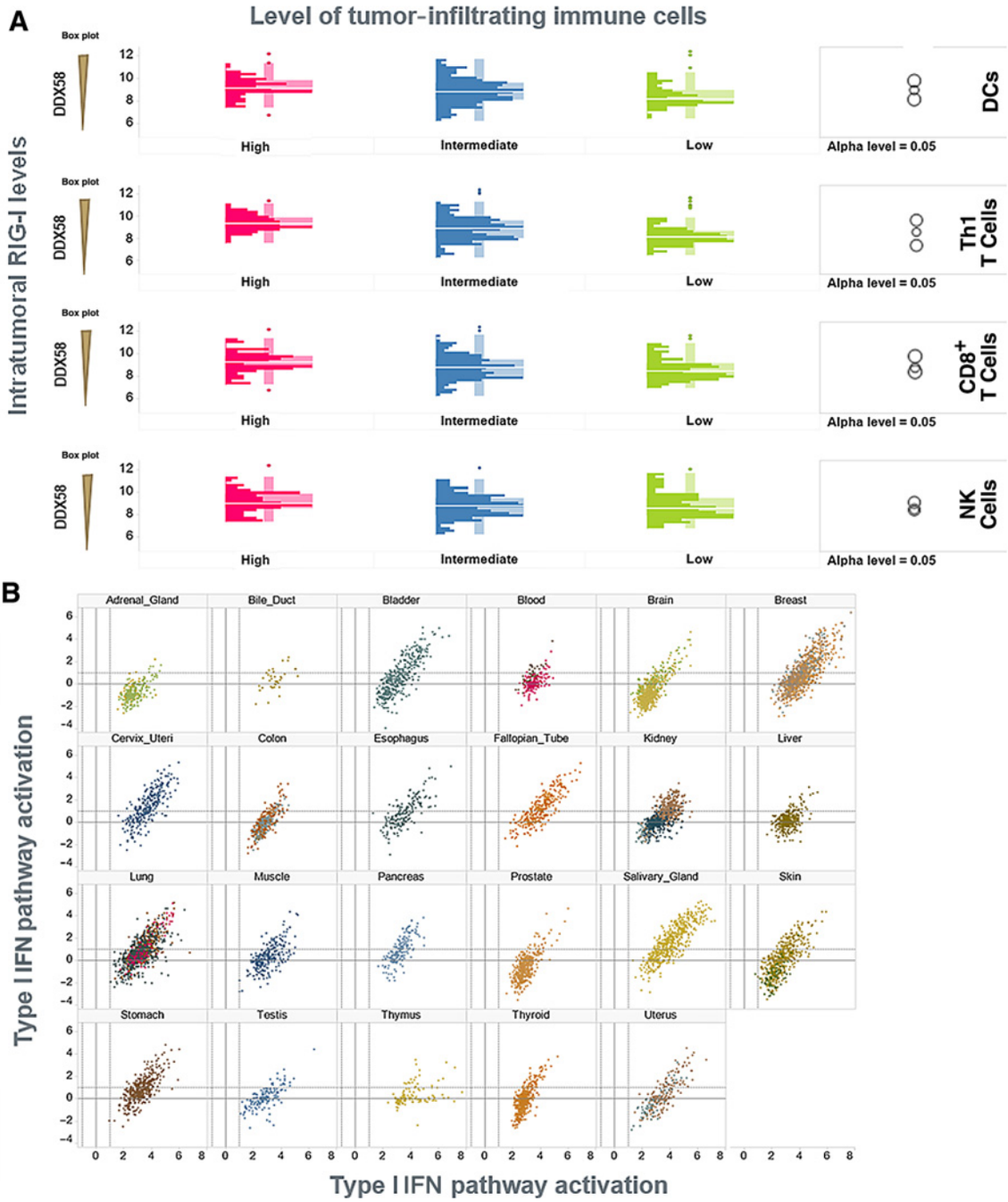

Figure 1.

RIG-I (DDX58) expression correlates with immune cell infiltration signatures and type I IFN pathway activation. **A,** RIG-I mRNA expression levels were compared in tumor groups classified by levels of immune cell infiltration as indicated on the basis of GSVA data. Graphical representation of Student *t* test analysis (right) shows significant differences between "high" and "low" groups for dendritic cells and Th1 T cells by means of nonoverlapping circles. **B,** Type I IFN pathway activation and RIG-I gene expression are positively correlated across tumors of all tested tissue origin, including skin.

Human melanoma is responsive to treatment with RIG-I agonist ppp-RNA *in vitro*

To further corroborate the potential of ppp-RNA as a therapeutic modality for human melanoma, we tested a panel of melanoma cell lines for their response to treatment with synthetic tool ppp-RNA molecules *in vitro*. Because the data obtained from human tumor material was only available on the RNA level, we followed up by quantification of expression of selected proteins [IP-10, PD-L1, FasR and (NK-cell ligand) MHC-I] in response to ppp-RNA (Figs. 2 and 3; Supplementary

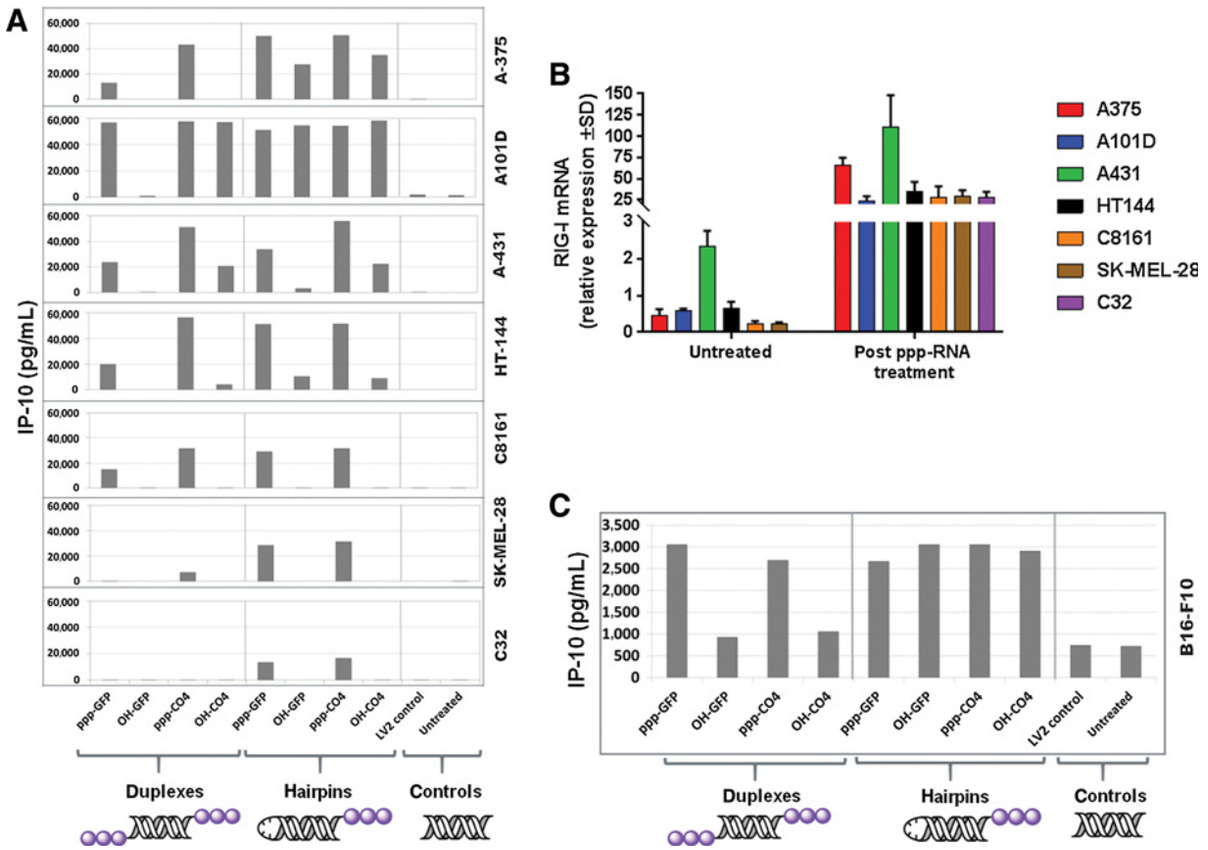

Figure 2.

Cell line response to RIG-I treatment. **A,** Response profile of a panel of human melanoma cell lines after treatment with RIG-I agonist ppp-RNA and respective controls at 100 nmol/L. IP-10 concentration in supernatant was quantified as surrogate for type I IFN response 48 hours posttreatment by reverse transfection with synthetic ppp-RNA and respective OH-RNA controls as indicated. **B,** Response profile of a panel of human melanoma cell lines pre- and posttreatment with RIG-I agonist ppp-RNA (CO4 hairpin) at 100 nmol/L. Relative expression of RIG-I (DDX58) mRNA was quantified by qRT-PCR. **C,** Response profile of murine B16-F10 cells after treatment with RIG-I agonist ppp-RNA and respective controls at 100 nmol/L. IP-10 concentration in supernatant was quantified as surrogate for type I IFN response 48 hours posttreatment by reverse transfection with synthetic ppp-RNA and respective OH-RNA controls as indicated.

Fig. S5). To take into consideration the impact of the sequence of ppp-RNA on RIG-I activation, we used two different sequences ("CO4" and "GFP"). Furthermore, because many publications on ppp-RNA activity used *in vitro* transcription (IVT) for generation of ppp-RNA, we sought to control for the potential role of hairpin structures (as resulting from single-reaction IVT protocols) in RIG-I activation.

The level of RIG-I activation was assessed by quantification of IP-10 (Fig. 2A) and confirmed at the level of IFNβ and RIG-I feedback loop upregulation by mRNA qPCR (Supplementary Fig. S4). Most importantly, we were able to elicit activation of IP-10 by ppp-RNA treatment in all of the tested cell lines, indicating general utility of a therapeutic ppp-RNA treatment approach in human melanoma. However, strong differences in response profiles were observed between the tested cell lines: While some cell lines, like C32 and SK-MEL-28, reacted almost exclusively to hairpin structured ppp-RNAs (and with only low-level responses), other cell lines (particularly A101D, A-375, and A-431) behaved much more promiscuously with regard to structure, ppp-tail and sequence. In addition, the hairpin-containing RNAs elicited triphosphate-independent responses in 4 of 7 cell lines regardless of the sequence, while for the duplex-RNA only the CO4 sequence displayed activity in the OH variant (in 3 of 7 cell lines). To assess whether the baseline RIG-I expression plays a role for the treatment response in our melanoma cell panel, we checked RIG-I mRNA levels pre- ("baseline") and posttreatment with ppp-RNA (Fig. 2B). On the basis of these data, a Pearson correlation analysis indicated a weak, but significant positive correlation between base levels and posttreatment response ($r^2 = 0.6594$, $P < 0.05$). When aligned with the IP-10 protein response data, it is notable that the poorest responder (C32) is the cell line with the lowest RIG-I mRNA baseline levels. Similarly, the other low-level responders (SK-MEL-28, C8161) are also characterized by relatively low RIG-I mRNA baseline levels. However, on the other hand, the most promiscuous responder (A101D) did not stand out by particularly high mRNA base levels. Vice versa, the cell line with the highest RIG-I mRNA levels (A-431) was only mildly promiscuous in its ppp-RNA response.

Before embarking on *in vivo* studies in murine syngeneic tumor models, we confirmed that the chosen mouse melanoma cell line (B16-F10) also responded to ppp-RNA treatment (Fig. 2C). Similarly to the human A101D cells, B16-F10 responded to hairpin

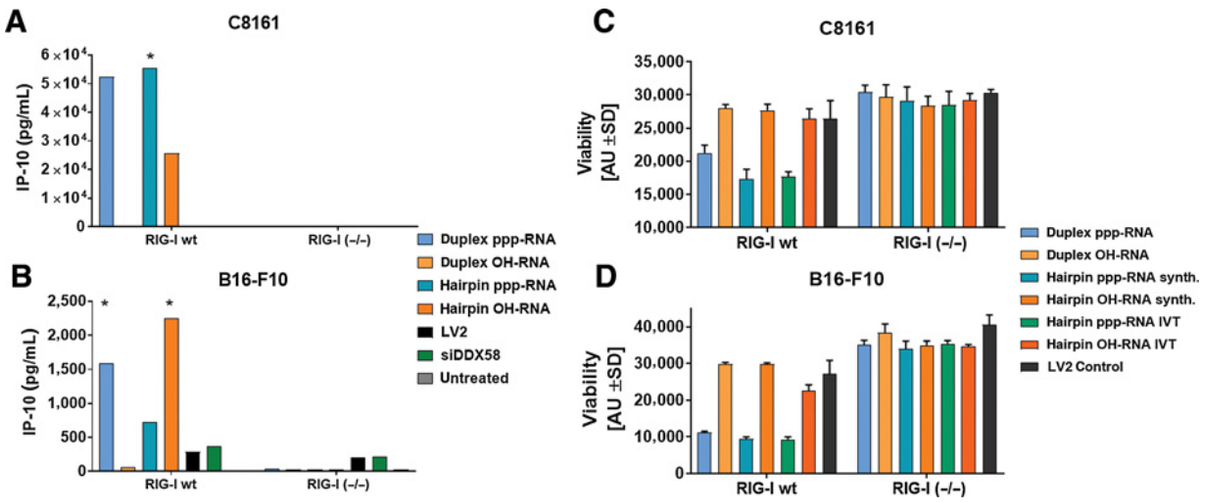

Figure 3.

Comparison of RIG-I wild-type and knockout cell variants following treatment with ppp-RNA. Analysis of IP-10 secretion following RNA treatment of C8161 (**A**) and B16-F10 (**B**) parental cells and a representative CRISPR/Cas–generated KO clone. Cells were treated with RIG-I agonist ppp-RNA and respective controls at 100 nmol/L. IP-10 concentration in supernatant was quantified as surrogate for type I IFN response 48 hours posttreatment by reverse transfection with synthetic ppp-RNA and respective OH-RNA controls as indicated. RIG-I knockout variants are characterized by absence of RIG-I agonist–triggered IP-10 secretion (asterisk indicates visible cell death in respective culture wells). Analysis of cell viability following RNA treatment of parental and KO variants of C8161 (**C**) and B16-F10 (**D**). Cells were treated with ppp-RNA variants and respective controls at 100 nmol/L and viability assessed 68 hours posttreatment.

RNA independent of the triphosphate by IP-10 induction, but was selective when treated with duplex RNA (as used *in vivo*), where only the triphosphate variants induced IP-10 induction above background. Collectively, these results demonstrate induction of type I IFN signaling in human and mouse melanoma cells upon treatment with RIG-I agonist ppp-RNA.

Type I IFN response and cytotoxic effect of ppp-RNA treatment is RIG-I dependent

To confirm that the type I IFN response and cytotoxic effects conferred by RIG-I agonist ppp-RNA are mediated exclusively via RIG-I, we created RIG-I knockout cell lines based on human C8161 and murine B16-F10 cells using CRISPR/Cas technology. We found that all ppp-RNA triggered effects on IP10 protein and IFNβ and RIG-I mRNA feedback induction, are abrogated in the KO cell lines (IP-10 secretion shown in Fig. 3A and B, IFNβ and RIG-I mRNA in Supplementary Fig. S4). Notably, this was also true for the effects that we observed after treatment with the hairpin-OH-RNA control, indicating, that the triphosphate-independent treatment effects are fully dependent on RIG-I and are not transmitted via an alternative receptor. The RIG-I knockout clones were furthermore analyzed for their sensitivity to cytotoxic effects of ppp-RNA treatment in a viability assay (Fig. 3C and D). As with the IFN response, all cytotoxic effects of ppp-RNA observed in the parental wild-type cells were abrogated by knocking out RIG-I in both human and mouse cell lines. Finally, we examined additional cellular responses, which were reported as ppp-RNA/RIG-I dependent (15). To this end, we performed flow cytometry analysis of membrane expression of MHC-I, PD-1L, and FasR (CD95) following the treatment with ppp-RNA and with the respective controls (Supplementary Fig. S5). While MHC-I and PD-1L were both induced by ppp-RNA compared with OH-RNA control regardless of the duplex or hairpin structure in wild-type cells, FasR was only weakly induced by the hairpin in human C8161 cells compared with mouse B16-F10 where FasR was induced independent of the RNA structure. In all cases, the effects observed after ppp-RNA treatment were completely abrogated in the KO cells, again indicating full dependency on RIG-I signaling for the treatment effects.

RIG-I agonist ppp-RNA triggers comprehensive immune activation and antitumor response in a syngeneic mouse melanoma model *in vivo*

Following the demonstration of treatment response of a panel of human melanoma cells and dependency of these observed effects on RIG-I *in vitro*, we carried out *in vivo* tumor studies to demonstrate therapeutic antitumor effect of ppp-RNA and further characterize the immune response triggered by treatment with this *bona fide* RIG-I agonist.

On the basis of the results of an exploratory *in vivo* study (Supplementary Fig. S6), we selected ppp-GFP for its strong IFN-stimulating effect. B16-F10 melanoma were implanted subcutaneously into both flanks of the mice. Only the left tumor on each mouse was injected intratumorally four times with 20 μg PEI-formulated ppp-GFP (Fig. 4A). In line with our *in vitro* results, we found a strong acute type I IFN serum response 6 hours posttreatment as indicated by high IFN-α levels compared with OH-RNA and PBS mock treatment controls (Fig. 4D; cytokine panel overview in Supplementary Fig. S7). Furthermore, FACS analysis of spleen immune cells at study take-down (day 9 posttreatment initiation) demonstrated significantly increased numbers of early activated immune cells (as illustrated for CD8 T cells and NK cells in Fig. 4E and F; full dataset in Supplementary Fig. S8). Immunohistologic assessment of caspase-3–positive cells within the tumors indicated a trend for increased frequency of apoptotic cells in the ppp-RNA–treated tumors compared with controls (Fig. 4G). Strong growth-inhibiting treatment

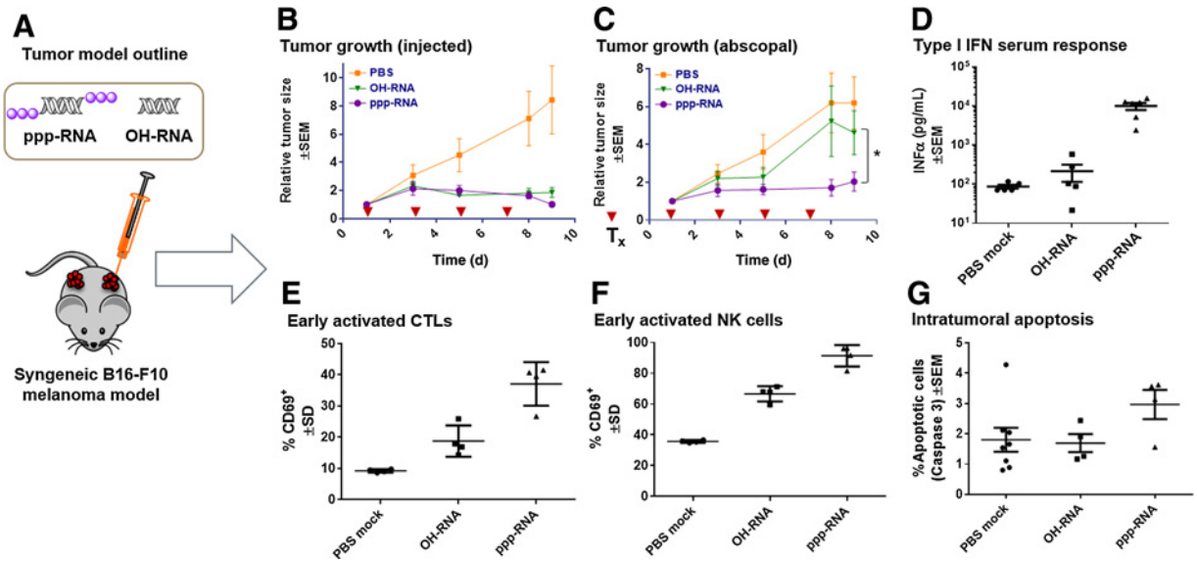

Figure 4.

Characterization of *in vivo* effects of intratumoral treatment of bilateral subcutanous B16-F10 tumors with ppp-RNA ("GFP"). **A,** Tumor model cartoon illustrating the treatment strategy, where only one of two implanted tumors is injected with ppp-RNA or the respective control ($n = 8$). **B,** Tumor growth chart showing the relative size of injected tumors following treatments on days 1, 3, 5, and 7. **C,** Tumor growth chart showing the relative size of apscopal tumors following treatments of the contralateral tumors on days 1, 3, 5, and 7 (*, $P < 0.05$). **D,** Type I IFN serum response illustrated by IFNα levels quantified from serum, taken from mice treated as indicated 6 hours post first intratumoral treatment. **E,** Fraction of early activated CTLs ($CD69^+$ relative to whole population) isolated from spleens at take down of mice treated as indicated. **F,** Fraction of early activated NK cells ($CD69^+$ relative to whole population) isolated from spleens at take down of mice treated as indicated. **G,** Fraction of apoptotic cells (indicated by caspase 3 positivity) in tumors based on histopathologic assessment dependent on treatments.

response was observed in the injected tumors compared with the PBS mock controls (Fig. 4B). Interestingly, the antitumor effect was only marginally stronger in the ppp-RNA–treated tumors compared with the OH-RNA–treated tumors, despite the type I IFN response. Conversely, we observed significant differences between untreated abscopal tumors, where tumors from ppp-RNA treated mice were significantly smaller at take-down compared with tumors from OH-RNA–treated mice (Fig. 4C). This observation indicates a systemic antitumor response following local intratumoral injection.

Encouraged by this initial study, we went on to demonstrate the survival benefit for ppp-RNA–treated animals (Fig. 5). Because of the strong antitumor and immune-stimulating effects of the GFP-based OH-RNA control (Fig. 4), we instead used an alternative sequence ("CO4"), which was found to confer less ppp-independent effects in an exploratory study (Supplementary Fig. S6). We also included an additional control, where OH-CO4 was backbone-modified with 2′-OMe to abrogate TLR7/8-dependent immunostimulatory effects (33). Indeed, we found the immune stimulation profile of ppp-RNA in this setting much more distinguished from the controls than in the first study. Especially regarding serum levels of IFNα, IP-10, and IFNγ, the ppp-CO4–treated mice showed strong differences after treatment compared with the control groups (Fig. 5D). Interestingly, KC/GRO was the only cytokine, where we did not find significant differences between ppp-RNA and control RNA–treated mice. Furthermore, large intragroup variability was observed for the serum cytokine levels of ppp-RNA–treated mice. Therapeutic antitumoral effect was quantified by tumor size measurement and survival analysis (where 1,000 mm^3 was used as survival threshold value). While no animal showed complete tumor remission, Kaplan–Maier analysis demonstrated that ppp-RNA–treated animals had a significantly prolonged survival compared with the OH-RNA–treated animals. This observation is in line with the tumor growth data, where ppp-RNA–treated tumors were significantly smaller than control RNA–treated tumors and PBS controls on day 17 posttreatment (when the first animals were removed from the study for animal welfare reasons). OH-RNA and OH-2′OMe-RNA–treated groups were indistinguishable in tumor growth and survival.

Overall, the observed differences in tumor response between the groups were reflected at the level of acute cytokine responses 6 hours after the first intratumoral treatment: ppp-RNA–treated animals showed an almost exclusive response for most of the analyzed cytokines, including IP-10 and IFNα. Similar to tumor growth data, no significant difference was observed between OH-RNA and OH-2′OMe-RNA. KC/GRO and, to a lesser extent, IL6 were the only cytokines that were induced by all of the RNAs, but not by PBS injection.

Within the ppp-RNA group, IL10 and IP-10 responses correlate positively with survival and negatively with tumor size based on a Pearson correlation analysis (IL10 vs. tumor size: $r^2 = 0.44$, $P < 0.05$; IL10 vs. survival: $r^2 = 0.45$, $P < 0.05$; IP-10 vs. tumor size: $r^2 = 0.43$, $P < 0.05$; IP-10 vs. survival: $r^2 = 0.44$, $P < 0.05$). None of the other cytokines (including IFNα) showed such relationship. Taken together, these observations establish a role for ppp-RNA and RIG-I signaling in tumor growth control of both injected and non-injected (contralateral) mouse melanoma lesions.

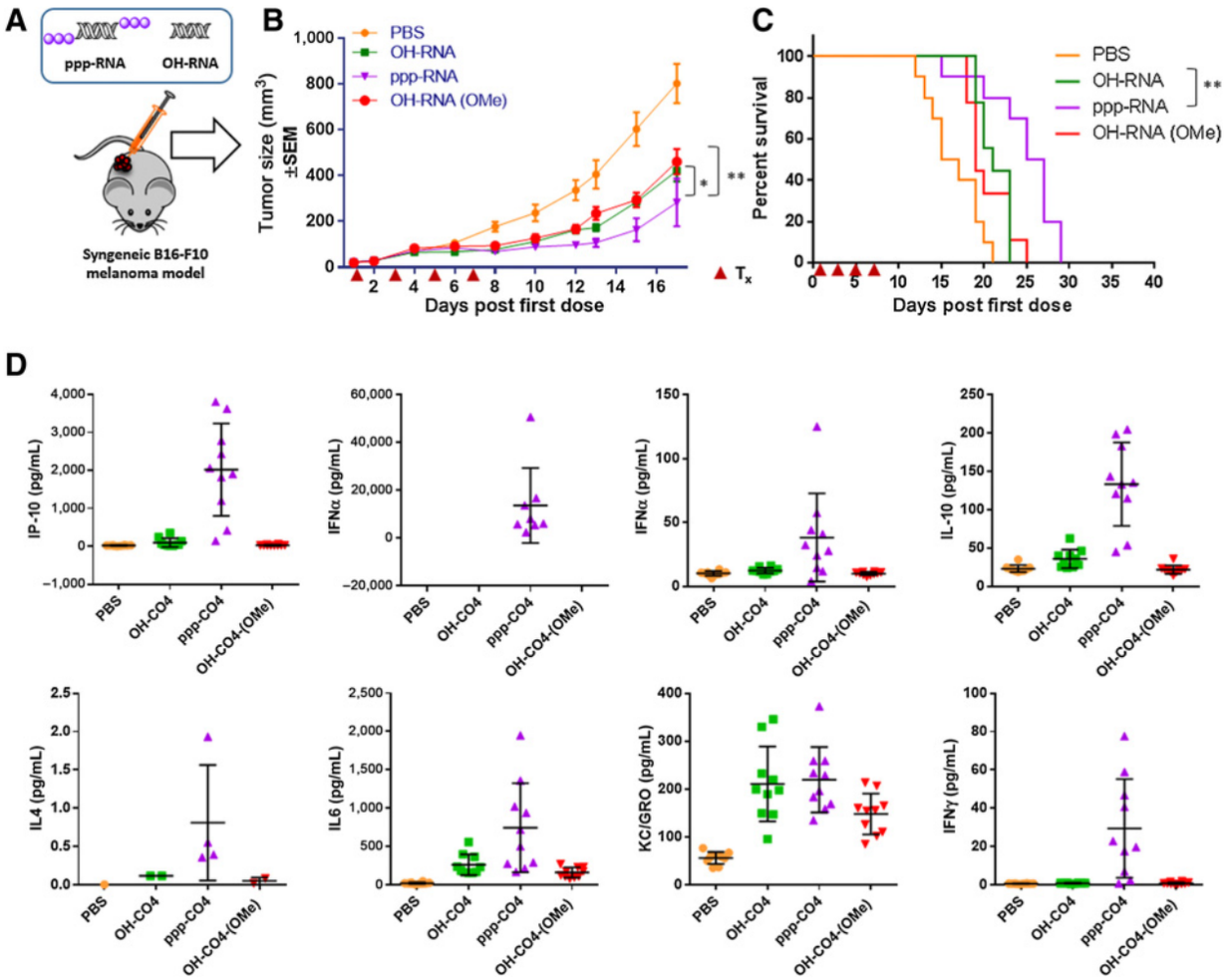

Figure 5.

Demonstration of prolonged survival after intratumoral treatment of unilateral subcutanous B16-F10 tumors with ppp-RNA ("CO4"). **A,** Tumor model cartoon illustrating the treatment strategy, where a single tumor is implanted and injected with ppp-RNA or the respective control ($n = 10$). **B,** Tumor growth chart showing the relative size of injected tumors following treatments on days 1, 3, 5, and 7. Tumor sizes were compared using a two-way ANOVA, including Tukey multiple comparison test (** indicates $P < 0.002$, * indicates $P < 0.033$). **C,** Kaplan–Meier plot, demonstrating a survival advantage of ppp-RNA–treated animals compared with the control groups. A tumor size of 1,000 mm^3 was used as threshold for survival. Mean survivals: PBS: 16 days, OH-RNA: 21 days, OH-RNA (OMe): 19 days, ppp-RNA: 26 days. Survival curves were compared using a log-rank test (**, $P < 0.01$). **D,** Serum cytokine response profile 6 hours post first intratumoral treatment. Error bars, SD.

RIG-I activation by ppp-RNA triggers an adaptive immune response

Following the demonstration of systemic antitumor effects and prolonged survival, we set up a tumor model to address the question, whether the observed systemic immune activation translated into an adaptive immune response involving tumor antigen–specific T-cell proliferation. To this end, we employed a variation of the B16-F10 model, where the tumor cells express OVA as a dominant tumor antigen (B16-OVA). After intratumoral treatment of this model with ppp-RNA and the respective controls, we found a significant increase in OVA-specific CD8 T cells in whole blood of these animals using OVA-specific tetramer staining method followed by FACS analysis (Fig. 6). Interestingly, the frequency of OVA-specific CD8 T cells was highly variable between animals despite four rounds of injection, which should rule out variations based on potential differences in intratumoral injection locations. The large T-cell response variability matches the variability observed for cytokine responses in this and our preceding *in vivo* studies. We observed a general correlation between serum cytokine levels and OVA-specific CTL activation in this model (Supplementary Fig. S9; Supplementary Table S2). While our data did not allow for a direct correlation of survival and OVA-specific CTLs, we observed a significant correlation between the induction of IP-10 and IL10 with antigen-specific T-cell response, which is in line with the survival study data. KC/GRO was the only cytokine that did not correlate with survival thus further stressing that it is likely unrelated to the ppp-RNA–specific systemic antitumor response (compare Fig. 5D). In summary, our data demonstrate that RIG-I activation by ppp-RNA leads to the development of tumor-specific adaptive immunity.

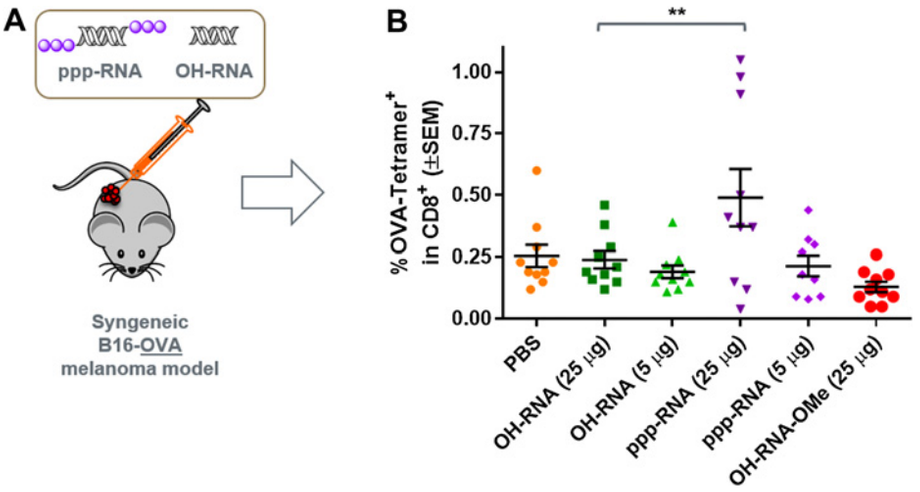

Figure 6.
Demonstration of a tumor antigen–specific CTL response after intratumoral treatment of subcutanous B16-OVA tumors with ppp-RNA (CO4 sequence). **A,** Tumor model cartoon illustrating the treatment strategy, where a single tumor is implanted and injected with ppp-RNA or the respective control ($n = 10$). **B,** Results of FACS analysis following an OVA-peptide–specific Tetramer staining to quantify the fraction of OVA-specific $CD8^+$ T cells in whole blood following treatments as indicated on *x*-axis. Fractions were compared using unpaired Student *t* test (**, $P < 0.01$).

Discussion

The goal of the presented work was to examine the potential of the RIG-I agonist ppp-RNA as a treatment option for cancer and to gain a better understanding of the advantages, limitations, and pitfalls of this approach. To this end, we attempted to obtain a comprehensive view of expression and functional consequences of RIG-I activation in patient tumor material, human tumor cell models, and *in vivo* tumor mouse models.

While previously published data suggested a protective role for RIG-I in liver cancer (34, 35), we focused on the immunologic implications of RIG-I expression levels in human cancers with a focus on melanoma as a possible entry indication for treatment via intratumoral drug administration. The most fundamental insight we gained from our tumor expression analyses is that available data support the assumption that the association of RIG-I expression with IFN-related pathway activation and immune cell infiltration are functional in the context of all examined tumor types, including melanoma. Unfortunately, RNA expression data hold limited information about the activation level of RIG-I protein. Furthermore, based on the paradigm that RIG-I activation and type I IFN response are connected via a feedback loop (36), no causative conclusions on this relationship can be drawn from our data. Therefore, while it is tempting to speculate that high RIG-I expression and concomitant activation might imply a better prognosis by providing a more immune-active tumor environment, currently available data do not support such hypothesis. Related to this, no data are currently available to judge the role of RIG-I as a biomarker for RIG-I agonist treatment response. While our (limited) tissue culture data obtained in human melanoma indicate a general positive correlation between RIG-I baseline levels and extent of IFN response, this cannot easily be translated to the tumor setting, where infiltrating immune cells and cytokines are important factors that are interrelated with RIG-I via feedback loops. Type I IFN is mainly produced by pDCs and macrophages, but also by somatic cells and tumor cells, while type II IFN is only secreted by NK/NKT and T cells in relevant concentrations. While IFN type I will be secreted upon injection of ppp-RNA already few hours later, IFN type II will only be produced upon activation of NK and T cells and may imply a positive correlation between IFN type I production and immune cell activation. Beside the integrity of the primary RIG-I-IFN axis in cancer, similarly encouraging are our observations showing that RIG-I expression correlates with gene expression signatures that indicate infiltration of T-cells, NK-cells and DCs. Again, causalities are unclear, but the data are compatible with the hypothesis that RIG-I activity in tumors can lead to the influx of immune cells, required for an effective antitumor immune response. In addition, the observation, that PD-L1 and PD-L2 are among the genes, which are most prominently coexpressed with RIG-I in tumors, underlines the complementary potential of a combination of immune checkpoint inhibitors and RIG-I agonist treatment. Our data also suggest that IFNβ might play a particular role in the RIG-I–associated IFN profile in the examined tumors. This would be in line with recent findings, suggesting, that IFNβ is associated with immune suppression including promotion of suppressive factors like PD-L1 (37).

Further to the human tumor data, our *in vitro* analyses of cultured human tumor cell lines show a general susceptibility of human melanoma to treatment with RIG-I agonist ppp-RNA as evidenced by upregulation of a type I IFN response and RIG-I feedback induction. However, our results also indicate a considerable heterogeneity of response across the tested cell lines with regard to both sensitivity and selectivity toward the agonist. Our data show that this heterogeneity is partly correlated with RIG-I mRNA baseline expression levels, implying that IFN pretreatment (to induce RIG-I expression) could enhance a RIG-I agonist treatment response. While the majority of cell lines respond to ppp-RNA regardless of the presence of a hairpin structure, we observed that the presence of a hairpin loop in the RNA is required in some instances to elicit a detectable response (e.g., SK-MEL-28 and C32). Furthermore, the presence of a hairpin loop in some (but not all) cell lines seems sufficient to elicit an IFN induction independent of a triphosphate (particularly in A-375 and A101D). For duplex RNAs, triphosphate-independent effects appear to be sequence dependent. While we did not systematically examine this, it would be plausible to speculate, that this effect is induced via sequence-dependent secondary structures. Regardless of the exact mechanism, our data obtained in RIG-I knockout variants of human and murine melanoma cells indicate that both, the triphosphate dependent and independent effects, are relayed through RIG-I. This finding holds up for all of the effects we studied in the context of the project triggered by

RIG-I activation: type I IFN response, cytotoxicity, MHC-I, PD-L1, and FasR upregulation. Our data are not suited to demonstrate exclusive signaling of ppp-RNA through RIG-I, but are well compatible with the idea of coreceptors that are involved in RIG-I signaling.

While the identity of potential ppp-RNA coreceptors remains unknown, a role for several known receptors is unlikely, based on the observations. The absence of cytokine induction (IP-10), upregulation of HLA-I and PD-L1 (Supplementary Fig. S5), and reduction in cell viability upon ppp-RNA treatment of RIG-I KO cells demonstrates that no other RLR or TLR3/7/8 receptors is triggered as all of these receptors would result in the secretion of IFN and IP-10. One exception is LGP2 that does not comprise a CARD domain necessary for interaction with its downstream adaptor MAVS and initiation of a signaling cascade. It is established that LGP2 only modulates MDA-5 and RIG-I signaling (38) and has recently been associated with the argonaute siRNA machinery (39). In addition, TLR7 and 8 are not expressed in somatic cells and tumor cells (38, 40), but only on immune cells. The involvement of PKR, OAS/RNAseL, and the NLRP-inflammasome cannot be completely excluded, but as activation of these receptors ultimately leads to translational inhibition and cell death, which we do not detect in RIG-I KO cells, an involvement is unlikely.

In vivo, we also expect the RNAs to be detected by immune cells and there TLR7 and 8 may play a role in its recognition. The effect is controlled for by using a sequence-matched OH-RNA, which is not recognized by RIG-I, but may be recognized by other receptors like TLRs. Furthermore, a 2′-O–methylated OH-RNA was used that lacks recognition by TLRs to control for the TLR recognition. Figure 4B demonstrates that the OH-RNA has a direct positive effect on tumor control in the treated tumor, but lacks an effect on the abscopal tumor compared with ppp-RNA. We deliberately take into account that the activation of TLRs by ppp-RNA may have an additional therapeutic effect, but the activation of RIG-I is shown to be superior with regard to tumor control. We control for this effect by using the respective OH-RNAs.

Triphosphate and a blunt-ended base-paired region at the 5′-end have been described as the basic requirements for an efficient RIG-I agonist (20, 23, 41), while nontriphosphate dsRNA have been described as a less potent agonist (21, 42). Sequence composition was found to impact RIG-I activation in a largely obscure manner (43). Secondary structures have been convincingly described to contribute to RIG-I activation or even make a triphosphate obsolete (44–46). Our observations are consistent with these reports, but additionally show that the contribution of triphosphate moiety, RNA sequence, and hairpin structure on RIG-I–mediated effects are strongly dependent on the cellular background. This implies that for therapeutic applications of a RIG-I RNA agonist, much attention must be given to these features to target the maximal number of tumor cells in heterogeneous tumors or metastatic disease. It furthermore hints, that the integration of a target-specific RNAi-effect is likely to interfere considerably with the activity of sequence-optimized RIG-I agonists if the development of bifunctional therapeutic molecules is intended. This is due to conflicting sequence requirements for RIG-I agonism and siRNA-mediated target knockdown. In addition, current chemical modification strategies for nuclease protection of therapeutic siRNA may potentially interfere with RIG-I activation, which is a major concern for linking RIG-I–activating siRNAs to targeting moieties without protective encapsulation (20).

Our *in vivo* tumor data are in line with the literature reports demonstrating antitumoral effects in injected and abscopal tumors following intratumoral administration of ppp-RNA (14, 18, 19). We were able to corroborate the hallmarks of postulated mechanisms, including type I IFN response, tumor cell apoptosis, and activation of an innate and adaptive cellular immune response. At the same time, we found unexpectedly strong antitumoral effect of our OH-RNA controls, which is hardly discernable from ppp-RNA in the injected tumor, but can be significantly differentiated in abscopal tumors. The immunostimulatory effect of control OH-RNAs is also reflected on the level of CTL and NK-cell activation, but surprisingly less on IFNα level. In contrast to our data, much of the literature reports used IVT-generated ppp-RNA, where no matching OH-RNA control was available to properly control for such effects. Our findings therefore underline the need for synthetic RNA molecules for well-controlled development of therapeutic ppp-RNA molecules with clear mechanism of action. Of at least equal importance for therapeutic development in this context is the superior chemical purity that is generally achieved with synthetic RNA compared with IVT-derived material. Recapitulating our *in vitro* results, our independent *in vivo* studies further highlight sequence-dependent effects of the RNAs based on the differential intratumoral effects of CO4 and GFP sequence OH-RNAs. Our observation that 2′-OMe-modifications of the partially active OH-RNA control have no measurable effect on antitumor activity indicates that the observed effects are probably not based on TLR7 activity, which should be abrogated by this chemical modification. The cytokine profile obtained from our animal study points toward an association of KC/GRO or (to a lesser extent) IL6 with the OH-RNA effects, because these were the only cytokines in our panel that were significantly induced by all RNAs, but not in the PBS group. Overall, these findings argue that the frequently reported immunogenic/adjuvant effect of PEI (47–49) could play a considerable role in the antitumor effect of RNA-RIG-I agonist treatment via a mechanism that needs further clarification. An important aspect in this context is also the cell tropism of PEI delivery. So far, dendritic cells and tumor cells are considered to be target cell types initiating the primary IFN response to PEI-formulated ppp-RNA treatment (15, 19). It could be beneficial to study the effect of alternative delivery formulations to alter the cell targeting profile to include additional cell types including macrophages (50).

While we were able to confirm the mechanistic hallmarks of a RIG-I agonist–triggered response in a mouse tumor model, the overall antitumor efficacy we observed was only partial. Tumor growth, both locally and abscopally, was significantly reduced and survival prolonged. However, these effects were only temporary and all animals eventually succumbed to the tumor burden. While our ppp-RNAs were nonoptimized tool compounds tested in a rather aggressive tumor model, our data suggest that extended optimization effort is required to develop ppp-RNAs with sustained clinical treatment effects. Furthermore, ppp-RNA might strongly benefit from combination treatment (including checkpoint inhibitors) to achieve significant therapeutic benefit, as is the case for other PRR-targeted therapeutics (6, 7).

Notably, we demonstrated for the first time the systemic presence of tumor antigen–specific $CD8^+$ T cells following ppp-RNA treatment of a tumor model. While a general activation

of adaptive immune cells and CTL cross-priming has been demonstrated before (15, 18, 19, 50), our findings provide mechanistic confirmation of antigen-specific effects, fundamental for systemic and specific antitumor effects, required for eradication of metastatic disease. This observation alleviates concerns regarding suboptimal RNA delivery to limited tumor cell populations because, in principle, it should not be necessary to deliver ppp-RNA to all tumor cells, but only to a fraction for triggering the initial adaptive response and releasing tumor-specific antigens for T-cell priming.

Interestingly, we observed strong heterogeneity in the frequency of antigen-specific $CD8^+$ T cells between the ppp-RNA–treated animals, which was similarly observed in the cytokine profiles from all tumor studies. While in the OVA study all measured cytokines (except KC/GRO) showed at least borderline correlation with OVA-specific $CD8^+$ T-cell frequency, only IP-10 and IL10 (which also stand out in the OVA study) were correlated with survival and tumor response. While this was expected for IP-10 due to its central role in type I IFN response, IL10 has not been directly implicated yet in RIG-I–mediated antitumor effects. It has been described to be secreted by DCs via IRF-3–dependent RIG-I signaling in antiviral response (51). While early reports on IL10 highlight its anti-inflammatory and immunosuppressive functions, which could contribute to an immune-suppressive tumor environment (52–55), a more complex biology and significant antitumor activity has emerged over the last years (56–58). A possible mechanism for this effect is that IL-10 directly induces specific activation and expansion of tumor-resident $CD8^+$ T cells (59). While this is a plausible explanation, its potential to suppress T lymphocyte activities through downregulation of antigen presentation by APCs and direct inhibition of T-cell proliferation would be in conflict with the assumed mechanisms of a RIG-I–triggered type I IFN response as basis for the antitumor activity of ppp-RNA. Further investigation on the role of IL-10 in RIG-I–mediated tumor therapy could bring meaningful insight.

Because we performed four repeated injections in each tumor at different time points and intratumoral locations, it seems unlikely, that the described intragroup heterogeneity is simply due to injections into different tumor compartments or necrotic regions. The observations could, in fact, reflect varying propensities of tumors and their microenvironment to respond to the treatment. This might have implications and limitations also for clinical applications and underlines the need for the identification of biomarkers and predictors of treatment response, which is an open task to date. While a basic expression of functional RIG-I within a tumor likely is a prerequisite to a ppp-RNA treatment response, it is unlikely that simple expression levels have much predictive power, because RIG-I expression upregulation can be triggered by IFN signaling and ppp-RNA treatment. Thus, therapeutic ppp-RNA treatment might work equally well on tumors where RIG-I levels are already upregulated by a type I IFN environment and on tumors where levels are only upregulated via feedback induction following agonist treatment initiation. RIG-I is known to be an IFN-stimulated gene itself, but its activation also leads to the induction of IFN. This fact is beneficial for the therapy and states an important self-amplifying feedforward loop that is well recognized in literature (60). After RIG-I stimulation, the secreted IFN acts in an autocrine and paracrine manner to modulate the expression of many hundred genes on a transcriptome and proteome level (61) including RIG-I to initiate an appropriate immune response.

While in our nonexhaustive analysis of melanoma cell lines *in vitro*, there was a mild correlation between baseline RIG-I levels and response levels, this likely has limited significance in the complex tumor environment where immune cells (particularly DCs) and cytokines contribute to the response. Further work is required to elucidate the regulatory biology of RIG-I and identify critical and predictive components of the associated pathways to identify patients that could benefit most from a RIG-I agonist treatment.

In summary, we present comprehensive data validating the concept of intratumoral cancer treatment with synthetic RIG-I agonist ppp-RNA, while highlighting challenges and open questions. In brief, we have demonstrated that clinical mRNA expression data overall support the concept of tumoral activation of RIG-I in a wide variety of tumor types including melanoma. Furthermore, cellular models of human melanoma confirm *in vitro* and *in vivo* susceptibility to ppp-RNA treatment. We demonstrate RIG-I dependency of ppp-RNA–triggered effects and highlight the impact of RNA features and cellular background for treatment response. For the first time, we demonstrate systemic presence of tumor antigen–specific CTLs following treatment with RIG-I agonist.

ppp-RNA and analogues thereof have the potential to play an important role for cancer treatment in the next wave of immunotherapy. However, a number of challenges in the generation and formulation of potent agonists must still be solved. Similarly, a deeper understanding of the biology and regulation of RIG-I are critical for its clinical utility.

Disclosure of Potential Conflicts of Interest

M.W. Helms is an employee of Sanofi. K. Jahn-Hofmann is a section head at Sanofi. K. Grandien is a senior research scientist/employee at Sanofi. J. Theilhaber is a scientist at Sanofi. T.R. Wagenaar is an employee at Sanofi. S. Endres reports receiving a commercial research grant from Sanofi. D. Wiederschain is a global head of IO research at Sanofi. S. Rothenfußer reports receiving a commercial research grant from Sanofi. B. Brunner is a research scientist at Sanofi. L.M. König reports receiving a commercial research grant from Sanofi. C. Metz-Weidmann, M. Braun, G. Dietert, P. Scherer, H. Cao are all employees of Sanofi. F. Gnerlich is an employee of AstraZeneca. No potential conflicts of interest were disclosed by the other authors.

Authors' Contributions

Conception and design: M.W. Helms, K. Jahn-Hofmann, F. Gnerlich, M. Braun, T.R. Wagenaar, S. Endres, D. Wiederschain, S. Scheidler, S. Rothenfußer, B. Brunner, L.M. König

Development of methodology: M.W. Helms, K. Jahn-Hofmann, M. Braun, L.M. König

Acquisition of data (provided animals, acquired and managed patients, provided facilities, etc.): M.W. Helms, F. Gnerlich, C. Metz-Weidmann, M. Braun, K. Grandien, B. Brunner

Analysis and interpretation of data (e.g., statistical analysis, biostatistics, computational analysis): M.W. Helms, M. Braun, G. Dietert, K. Grandien, J. Theilhaber, H. Cao, S. Rothenfußer, B. Brunner, L.M. König

Writing, review, and/or revision of the manuscript: M.W. Helms, M. Braun, G. Dietert, K. Grandien, H. Cao, M.M. Schnurr, D. Wiederschain, S. Scheidler, S. Rothenfußer, B. Brunner, L.M. König

Administrative, technical, or material support (i.e., reporting or organizing data, constructing databases): M.W. Helms, K. Jahn-Hofmann, P. Scherer, M.M. Schnurr, B. Brunner

Study supervision: M.W. Helms, D. Wiederschain

Other (design and synthesis of RIG-I agonists): F. Gnerlich

Acknowledgments

The study was supported by grants from Deutsche Forschungsgemeinschaft (DFG RO 2525/5-1, to S. Rothenfußer; DFG SCHN 664/5-1, to M.M. Schnurr), the international doctoral program "i-Target: Immunotargeting of cancer" funded by the Elite Network of Bavaria (to M.M. Schnurr, L.M. König, and S. Endres), and Else Kröner-Fresenius-Stiftung (2017_A50, to L.M. König).

The costs of publication of this article were defrayed in part by the payment of page charges. This article must therefore be hereby marked *advertisement* in accordance with 18 U.S.C. Section 1734 solely to indicate this fact.

Received November 13, 2018; revised April 5, 2019; accepted September 6, 2019; published first September 12, 2019.

References

1. Pico de Coana Y, Choudhury A, Kiessling R. Checkpoint blockade for cancer therapy: revitalizing a suppressed immune system. Trends Mol Med 2015;21:482–91.
2. Yang Y. Cancer immunotherapy: harnessing the immune system to battle cancer. J Clin Invest 2015;125:3335–7.
3. Teng MW, Ngiow SF, Ribas A, Smyth MJ. Classifying cancers based on T-cell infiltration and PD-L1. Cancer Res 2015;75:2139–45.
4. Tumeh PC, Harview CL, Yearley JH, Shintaku IP, Taylor EJ, Robert L, et al. PD-1 blockade induces responses by inhibiting adaptive immune resistance. Nature 2014;515:568–71.
5. Sharma P, Allison JP. Immune checkpoint targeting in cancer therapy: toward combination strategies with curative potential. Cell 2015;161:205–14.
6. Minn AJ, Wherry EJ. Combination cancer therapies with immune checkpoint blockade: convergence on interferon signaling. Cell 2016;165:272–5.
7. Junt T, Barchet W. Translating nucleic acid-sensing pathways into therapies. Nat Rev Immunol 2015;15:529–44.
8. Schlee M. Master sensors of pathogenic RNA - RIG-I like receptors. Immunobiology 2013;218:1322–35.
9. Wu J, Chen ZJ. Innate immune sensing and signaling of cytosolic nucleic acids. Annu Rev Immunol 2014;32:461–88.
10. Huen AO, Rook AH. Toll receptor agonist therapy of skin cancer and cutaneous T-cell lymphoma. Curr Opin Oncol 2014;26:237–44.
11. Lara PN Jr, Douillard JY, Nakagawa K, von Pawel J, McKeage MJ, Albert I, et al. Randomized phase III placebo-controlled trial of carboplatin and paclitaxel with or without the vascular disrupting agent vadimezan (ASA404) in advanced non-small-cell lung cancer. J Clin Oncol 2011;29:2965–71.
12. Conlon J, Burdette DL, Sharma S, Bhat N, Thompson M, Jiang Z, et al. Mouse, but not human STING, binds and signals in response to the vascular disrupting agent 5,6-dimethylxanthenone-4-acetic acid. J Immunol 2013;190:5216–25.
13. Gao P, Ascano M, Zillinger T, Wang W, Dai P, Serganov AA, et al. Structure-function analysis of STING activation by c[G(2′,5′)pA(3′,5′)p] and targeting by antiviral DMXAA. Cell 2013;154:748–62.
14. Besch R, Poeck H, Hohenauer T, Senft D, Hacker G, Berking C, et al. Proapoptotic signaling induced by RIG-I and MDA-5 results in type I interferon-independent apoptosis in human melanoma cells. J Clin Invest 2009;119:2399–411.
15. Duewell P, Steger A, Lohr H, Bourhis H, Hoelz H, Kirchleitner SV, et al. RIG-I-like helicases induce immunogenic cell death of pancreatic cancer cells and sensitize tumors toward killing by CD8(+) T cells. Cell Death Differ 2014;21:1825–37.
16. Kaneda Y. The RIG-I/MAVS signaling pathway in cancer cell-selective apoptosis. Oncoimmunology 2013;2:e23566.
17. Schnurr M, Duewell P. Breaking tumor-induced immunosuppression with 5′-triphosphate siRNA silencing TGFbeta and activating RIG-I. Oncoimmunology 2013;2:e24170.
18. Ellermeier J, Wei J, Duewell P, Hoves S, Stieg MR, Adunka T, et al. Therapeutic efficacy of bifunctional siRNA combining TGF-beta1 silencing with RIG-I activation in pancreatic cancer. Cancer Res 2013;73:1709–20.
19. Poeck H, Besch R, Maihoefer C, Renn M, Tormo D, Morskaya SS, et al. 5′-Triphosphate-siRNA: turning gene silencing and Rig-I activation against melanoma. Nat Med 2008;14:1256–63.
20. Hornung V, Ellegast J, Kim S, Brzozka K, Jung A, Kato H, et al. 5′-Triphosphate RNA is the ligand for RIG-I. Science 2006;314:994–7.
21. Kato H, Takeuchi O, Mikamo-Satoh E, Hirai R, Kawai T, Matsushita K, et al. Length-dependent recognition of double-stranded ribonucleic acids by retinoic acid-inducible gene-I and melanoma differentiation-associated gene 5. J Exp Med 2008;205:1601–10.
22. Wang Y, Ludwig J, Schuberth C, Goldeck M, Schlee M, Li H, et al. Structural and functional insights into 5′-ppp RNA pattern recognition by the innate immune receptor RIG-I. Nat Struct Mol Biol 2010;17:781–7.
23. Schlee M, Roth A, Hornung V, Hagmann CA, Wimmenauer V, Barchet W, et al. Recognition of 5′ triphosphate by RIG-I helicase requires short blunt double-stranded RNA as contained in panhandle of negative-strand virus. Immunity 2009;31:25–34.
24. Malissen N, Grob JJ. Metastatic melanoma: recent therapeutic progress and future perspectives. Drugs 2018;78:1197–209.
25. Hanzelmann S, Castelo R, Guinney J. GSVA: gene set variation analysis for microarray and RNA-seq data. BMC Bioinformatics 2013;14:7.
26. The Cancer Genome Atlas Research Network. Genomic classification of cutaneous melanoma. Cell 2015;161:1681–96.
27. Bindea G, Mlecnik B, Tosolini M, Kirilovsky A, Waldner M, Obenauf AC, et al. Spatiotemporal dynamics of intratumoral immune cells reveal the immune landscape in human cancer. Immunity 2013;39:782–95.
28. Theilhaber J, Rakhade SN, Sudhalter J, Kothari N, Klein P, Pollard J, et al. Gene expression profiling of a hypoxic seizure model of epilepsy suggests a role for mTOR and Wnt signaling in epileptogenesis. PLoS One 2013;8:e74428.
29. Surpris G, Chan J, Thompson M, Ilyukha V, Liu BC, Atianand M, et al. Cutting edge: novel Tmem173 allele reveals importance of STING N terminus in trafficking and type I IFN production. J Immunol 2016;196:547–52.
30. Sipes NJ, Bregman MD, Meyskens FL Jr. Stimulation of human metastatic melanoma colony-forming cells by an acid-sensitive factor in human platelet sonicate. Cancer Res 1985;45(12 Pt 1):6268–72.
31. Zlatev I, Manoharan M, Vasseur JJ, Morvan F. Solid-phase chemical synthesis of 5′-triphosphate DNA, RNA, and chemically modified oligonucleotides. Curr Protoc Nucleic Acid Chem 2012;Chapter 1:Unit1 28.
32. Wincott F, DiRenzo A, Shaffer C, Grimm S, Tracz D, Workman C, et al. Synthesis, deprotection, analysis and purification of RNA and ribozymes. Nucleic Acids Res 1995;23:2677–84.
33. Judge AD, Bola G, Lee AC, MacLachlan I. Design of noninflammatory synthetic siRNA mediating potent gene silencing in vivo. Mol Ther 2006;13:494–505.
34. Hou J, Zhou Y, Zheng Y, Fan J, Zhou W, Ng IO, et al. Hepatic RIG-I predicts survival and interferon-alpha therapeutic response in hepatocellular carcinoma. Cancer Cell 2014;25:49–63.
35. Liu Z, Dou C, Jia Y, Li Q, Zheng X, Yao Y, et al. RIG-I suppresses the migration and invasion of hepatocellular carcinoma cells by regulating MMP9. Int J Oncol 2015;46:1710–20.
36. Yoneyama M, Kikuchi M, Natsukawa T, Shinobu N, Imaizumi T, Miyagishi M, et al. The RNA helicase RIG-I has an essential function in double-stranded RNA-induced innate antiviral responses. Nat Immunol 2004;5:730–7.
37. Ng CT, Sullivan BM, Teijaro JR, Lee AM, Welch M, Rice S, et al. Blockade of interferon beta, but not interferon alpha, signaling controls persistent viral infection. Cell Host Microbe 2015;17:653–61.
38. Chow KT, Gale M Jr, Loo YM. RIG-I and other RNA sensors in antiviral immunity. Annu Rev Immunol 2018;36:667–94.
39. van der Veen AG, Maillard PV, Schmidt JM, Lee SA, Deddouche-Grass S, Borg A, et al. The RIG-I-like receptor LGP2 inhibits Dicer-dependent processing of long double-stranded RNA and blocks RNA interference in mammalian cells. EMBO J 2018;37. doi: 10.15252/embj.201797479.

40. Uhlen M, Fagerberg L, Hallstrom BM, Lindskog C, Oksvold P, Mardinoglu A, et al. Proteomics. Tissue-based map of the human proteome. Science 2015;347:1260419.
41. Schmidt A, Schwerd T, Hamm W, Hellmuth JC, Cui S, Wenzel M, et al. 5′-triphosphate RNA requires base-paired structures to activate antiviral signaling via RIG-I. Proc Natl Acad Sci U S A 2009;106:12067–72.
42. Takahasi K, Yoneyama M, Nishihori T, Hirai R, Kumeta H, Narita R, et al. Nonself RNA-sensing mechanism of RIG-I helicase and activation of antiviral immune responses. Mol Cell 2008;29:428–40.
43. Saito T, Owen DM, Jiang F, Marcotrigiano J, Gale M Jr. Innate immunity induced by composition-dependent RIG-I recognition of hepatitis C virus RNA. Nature 2008;454:523–7.
44. Hwang SY, Sun HY, Lee KH, Oh BH, Cha YJ, Kim BH, et al. 5′-Triphosphate-RNA-independent activation of RIG-I via RNA aptamer with enhanced antiviral activity. Nucleic Acids Res 2012;40:2724–33.
45. Xu J, Mercado-Lopez X, Grier JT, Kim WK, Chun LF, Irvine EB, et al. Identification of a natural viral RNA motif that optimizes sensing of viral RNA by RIG-I. MBio 2015;6:e01265–15.
46. Lee MK, Kim HE, Park EB, Lee J, Kim KH, Lim K, et al. Structural features of influenza A virus panhandle RNA enabling the activation of RIG-I independently of 5′-triphosphate. Nucleic Acids Res 2016;44:8407–16.
47. Shen C, Li J, Zhang Y, Li Y, Shen G, Zhu J, et al. Polyethylenimine-based micro/nanoparticles as vaccine adjuvants. Int J Nanomedicine 2017;12:5443–60.
48. Patnaik S, Gupta KC. Novel polyethylenimine-derived nanoparticles for in vivo gene delivery. Expert Opin Drug Deliv 2013;10:215–28.
49. Grant EV, Thomas M, Fortune J, Klibanov AM, Letvin NL. Enhancement of plasmid DNA immunogenicity with linear polyethylenimine. Eur J Immunol 2012;42:2937–48.
50. Hochheiser K, Klein M, Gottschalk C, Hoss F, Scheu S, Coch C, et al. Cutting edge: the RIG-I ligand 3pRNA potently improves CTL cross-priming and facilitates antiviral vaccination. J Immunol 2016;196:2439–43.
51. Samanta M, Iwakiri D, Takada K. Epstein-Barr virus-encoded small RNA induces IL-10 through RIG-I-mediated IRF-3 signaling. Oncogene 2008;27:4150–60.
52. de Waal Malefyt R, Haanen J, Spits H, Roncarolo MG, te Velde A, Figdor C, et al. Interleukin 10 (IL-10) and viral IL-10 strongly reduce antigen-specific human T cell proliferation by diminishing the antigen-presenting capacity of monocytes via downregulation of class II major histocompatibility complex expression. J Exp Med 1991;174:915–24.
53. de Waal Malefyt R, Yssel H, de Vries JE. Direct effects of IL-10 on subsets of human CD4+ T cell clones and resting T cells. Specific inhibition of IL-2 production and proliferation. J Immunol 1993;150:4754–65.
54. Halak BK, Maguire HC Jr, Lattime EC. Tumor-induced interleukin-10 inhibits type 1 immune responses directed at a tumor antigen as well as a non-tumor antigen present at the tumor site. Cancer Res 1999;59:911–7.
55. Taga K, Mostowski H, Tosato G. Human interleukin-10 can directly inhibit T-cell growth. Blood 1993;81:2964–71.
56. Moore KW, de Waal Malefyt R, Coffman RL, O'Garra A. Interleukin-10 and the interleukin-10 receptor. Annu Rev Immunol 2001;19:683–765.
57. Giovarelli M, Musiani P, Modesti A, Dellabona P, Casorati G, Allione A, et al. Local release of IL-10 by transfected mouse mammary adenocarcinoma cells does not suppress but enhances antitumor reaction and elicits a strong cytotoxic lymphocyte and antibody-dependent immune memory. J Immunol 1995;155:3112–23.
58. Berman RM, Suzuki T, Tahara H, Robbins PD, Narula SK, Lotze MT. Systemic administration of cellular IL-10 induces an effective, specific, and long-lived immune response against established tumors in mice. J Immunol 1996;157:231–8.
59. Emmerich J, Mumm JB, Chan IH, LaFace D, Truong H, McClanahan T, et al. IL-10 directly activates and expands tumor-resident CD8(+) T cells without de novo infiltration from secondary lymphoid organs. Cancer Res 2012;72:3570–81.
60. Schoggins JW, Wilson SJ, Panis M, Murphy MY, Jones CT, Bieniasz P, et al. A diverse range of gene products are effectors of the type I interferon antiviral response. Nature 2011;472:481–5.
61. Megger DA, Philipp J, Le-Trilling VTK, Sitek B, Trilling M. Deciphering of the human interferon-regulated proteome by mass spectrometry-based quantitative analysis reveals extent and dynamics of protein induction and repression. Front Immunol 2017;8:1139.